

Strong emission-line galaxies at low redshift in the field around the quasar SDSSp J104433.04–012502.2

Masaru AJIKI,¹ Yasuhiro SHIOYA,¹ Yoshiaki TANIGUCHI,¹ Takashi MURAYAMA,¹
Tohru NAGAO,^{2,3} Shunji S. SASAKI,¹ Ryoko SUMIYA,¹ Taichi MORIOKA,¹
Yuichiro HATAKEYAMA,¹ Asuka YOKOUCHI,¹ Mari I. TAKAHASHI,¹ and Osamu KOIZUMI¹

¹*Astronomical Institute, Graduate School of Science, Tohoku University,
Aramaki, Aoba, Sendai 980-8578*

²*INAF — Osservatorio Astrofisico di Arcetri,
Largo Enrico Fermi 5, 50125 Firenze, Italy*

³*National Astronomical Observatory,
Mitaka, Tokyo 181-8588, Japan*

(Received 2005 0; accepted 2005 0)

Abstract

We discuss observational properties of strong emission-line galaxies at low redshift found by our deep imaging survey for high-redshift Ly α emitters. In our surveys, we used the narrowband filter, *NB816* ($\lambda_{\text{center}} = 8150 \text{ \AA}$ with FWHM = 120 \AA), and the intermediate-band filter, *IA827* ($\lambda_{\text{center}} = 8270 \text{ \AA}$ with FWHM = 340 \AA). In this survey, 62 *NB816*-excess ($> 0.9 \text{ mag}$) and 21 *IA827*-excess ($> 0.8 \text{ mag}$) objects were found. Among them, we found 20 *NB816*-excess and 4 *IA827*-excess Ly α emitter candidates. Therefore, it turns out that 42 *NB816*-excess and 17 *IA827*-excess objects are strong emission-line objects at lower redshift. Since 4 objects in the two low- z samples are common, the total number of strong low- z emitters is 55. Applying our photometric redshift technique, we identify 7 H α emitters at $z \approx 0.24$, 20 H β -[OIII] ones at $z \approx 0.65$, and 11 [OII] ones at $z \approx 1.19$. However, we cannot determine reliable photometric redshifts of the remaining 17 emitters. The distributions of their rest frame equivalent widths are consistently understood with recent studies of galaxy evolution from $z \sim 1$ to $z \sim 0$.

Key words: galaxies : formation – galaxies : evolution – galaxies : high-redshift

1. Introduction

A number of deep imaging surveys for Ly α emitters (LAEs) at high redshift have been conducted in this decade, leading to the discovery of forming galaxies beyond $z = 5$ (see for review, Taniguchi et al. 2003b; Spinrad 2004). In these surveys, a narrowband filter with bandpass of $\sim 100 \text{ \AA}$ has been used. One of the most popular narrowband filters is a filter with the central wavelength of $\approx 8150 \text{ \AA}$, because OH airglow emission lines are significantly weak in this wavelength range. The use of this filter makes it possible to search for LAEs at $z \approx 5.7$ (Hu et al. 1999; Rhoads & Malhotra 2001; Ajiki et al. 2002, 2003; Taniguchi et al. 2003a; Hu et al. 2004; Wang, Malhotra, & Rhoads 2005; Ouchi et al. 2005; Westra et al. 2005).

In these surveys, strong emission-line objects such as starburst galaxies and active galactic nuclei (AGN) at low redshift can be also found (Stern et al. 2000; Fujita et al. 2003a; Ajiki et al. 2003, 2004; Hu et al. 2004); e.g., H α emitters at $z \approx 0.24$, [OIII] $\lambda 5007$ emitters at $z \approx 0.63$, [OIII] $\lambda 4959$ emitters at $z \approx 0.65$, H β emitters at $z \approx 0.68$, [OII] emitters at $z \approx 1.19$, and so on. It is important to estimate how many strong emission-line objects at low redshift (hereafter we call them strong low- z emitters) are present in such LAE searches and which kinds of strong low- z emitters are common. These strong low- z emitters have large emission-line equivalent widths since a typical survey limit of the rest-frame equivalent width for Ly α emitters at $z = 5.7$, 20 \AA corresponds to $\approx 135 \text{ \AA}$ for H α ones at $z = 0.24$, $\approx 100 \text{ \AA}$ for [OIII] ones at $z = 0.65$, and $\approx 61 \text{ \AA}$ for [OII] ones at $z = 1.19$.

In this paper, we investigate observational properties of such strong emission-line objects at low redshift found in our deep LAE survey with the narrowband filter, *NB816*, centered on 8150 \AA with the passband of $\Delta\lambda_{\text{FWHM}} = 120 \text{ \AA}$, and the intermediate-band filter, *IA827*, centered on 8270 \AA with the passband of $\Delta\lambda_{\text{FWHM}} = 340 \text{ \AA}$, that were carried out by using the prime-focus camera, Suprime-Cam on the 8.2 m Subaru Telescope (Ajiki et al. 2003, 2004).

In this paper, we adopt a flat universe with $\Omega_{\text{matter}} = 0.3$, $\Omega_{\Lambda} = 0.7$, and $H_0 = 70 \text{ km s}^{-1} \text{ Mpc}^{-1}$. Throughout this paper, magnitudes are given in the AB system.

2. Data

We have carried out an optical imaging survey for LAEs in the field surrounding the quasar SDSSp J104433.04–012502.2 at the redshift of 5.74 (Fan et al. 2000; Djorgovski et al. 2001; Goodrich et al. 2001), using the Suprime-Cam (Miyazaki et al. 2002) on the 8.2 m Subaru Telescope (Kaifu et al. 2000; Iye et al. 2004) on Mauna Kea. The Suprime-Cam consists of ten $2k \times 4k$ CCD chips and provides a very wide field of view, $34' \times 27'$ ($0.202 \text{ arcsec pixel}^{-1}$). In this survey, we used the narrowband filter, *NB816*, the intermediate band filter, *IA827*, and the broadband filters, *B*, *R_C*, *I_C*, and *z'*. The limiting magnitudes (3σ) within a 2.8-arcsec aperture of the reduced images are *NB816*= 26.0, *IA827*= 25.6, *B* = 26.6, *R_C* = 26.2, *I_C* = 25.9, and *z'* = 25.3. The total response (filter, optics, atmosphere transmission, and CCD

sensitivity are taken into account) curve of each filter is shown in figure 1. A summary of the imaging observations, source detection, and photometry are given in Ajiki et al. (2003, 2004).

3. Results and Discussion

3.1. *NB816*-selected sample of strong low- z emitters

As for *NB816*-excess objects, Ajiki et al. (2003) adopted the following criteria:

$$NB816 < 25.0 \tag{1}$$

and

$$Iz815 - NB816 > 0.9, \tag{2}$$

where *Iz815* is the continuum magnitude at $\lambda = 8150 \text{ \AA}$ estimated by using a combination of the flux densities (f_ν) in the I_C and z' bands;

$$f_{Iz815} = 0.76f_{I_C} + 0.24f_{z'}. \tag{3}$$

The *Iz815* magnitude gives us a good approximation of the continuum around 8150 \AA for the object without significant emission or absorption lines in the I_C and z' bands. There are 62 *NB816*-excess objects which satisfy the above two criteria.

In order to isolate LAE candidates from interlopers at lower redshift, they adopted the following criteria:

$$B > 26.6, \tag{4}$$

$$R_C - I_C > 1.8 \text{ for } I_C \leq 24.8, \tag{5}$$

and

$$R_C > 26.6 \text{ for } I_C > 24.8. \tag{6}$$

Then they obtained a final sample of 20 LAE candidates. Two objects were identified as LAEs at $z = 5.69$ and $z = 5.66$ from their follow-up optical spectroscopy (Ajiki et al. 2002; Taniguchi et al. 2003a).

Their analysis indicates that the remaining 42 objects are strong emission-line objects at lower redshift. Their properties are summarized in table 1. Their images and spectral energy distributions (SEDs) are shown in figure 2.

3.2. *IA827*-selected sample of strong low- z emitters

As for *IA827*-excess objects, Ajiki et al. (2004) adopted the following criteria:

$$IA827 < 24.9, \tag{7}$$

$$Iz827 - IA827 > 0.8, \tag{8}$$

and

$$Iz827 - IA827 > 3\sigma(Iz827 - IA827), \quad (9)$$

where $Iz827$ is the continuum magnitude at $\lambda = 8270 \text{ \AA}$ estimated by using a combination of the flux densities (f_ν) in the I_C and z' bands;

$$f_{Iz827} = 0.64f_{I_C} + 0.36f_{z'}. \quad (10)$$

The $Iz827$ magnitude gives us a good approximation of the continuum around 8270 \AA for the object without significant emission or absorption lines in the I_C and z' bands. There are 21 $IA827$ -excess objects which satisfy the above three criteria. In order to isolate LAE candidates from interlopers at lower redshift, they adopted the criteria of (4), (5), and (6). Finally they obtained a final sample of 4 LAE candidates.

Their analysis indicates that the remaining 17 objects are strong emission-line objects at lower redshift. Their properties are summarized in table 2. Their images and SEDs are shown in figure 3. Four of the 17 objects are common with $NB816$ -selected emitters, and the total number of strong low- z emitters is 55.

3.3. AGN fraction

As well as star forming galaxies, AGNs, especially broad-line (type 1) AGNs, also show strong emission lines. Therefore, we estimate a probable fraction of AGNs in our strong low- z emitter sample from a statistical point of view. Hao et al. (2005a) find 1317 broad-line AGNs from the Sloan Digital Sky Survey (SDSS; York et al. 2000). We use the catalog of their broad-line AGN sample which is available electronically, and find about 14% (1.2%), 4.5% (0.6%), and 1% (0.2%) of them satisfy the equivalent width criteria that correspond to those of our $NB816$ -($IA827$ -)selected $H\alpha$, $H\beta$ -[OIII], and [OII] emitters, respectively. Note that some of narrow line (type 2) AGNs satisfy our equivalent width criteria, although the fraction is negligibly small ($< 2\%$). On the other hand, we estimate the expected number of the AGNs in our $NB816$ -($IA827$ -) survey volume using AGN luminosity functions. Hao et al. (2005b) obtained the $H\alpha$, [OIII], and [OII] luminosity functions of the broad-line AGNs at $0 < z < 0.15$. Assuming their luminosity functions, we find that the expected numbers of AGNs in our $NB816$ ($IA827$) survey volume and luminosity range are 8.0 (6.2), 2.1 (1.4), and 0.2 (0.03), for the $H\alpha$, $H\beta$ -[OIII], and [OII] emitters, respectively. Assuming that there are no strong correlations between the equivalent widths and luminosities of AGNs, we combine these results and find that the total expected number of AGNs in our sample is ≈ 1 . Since this number is only $\approx 2\%$ of the total number of our strong low- z emitters, we ignore AGN contamination in the following analysis.

3.4. Classification of strong low- z emitters

Strong low- z emitters are considered to be $H\alpha$ emitters at $z \approx 0.24$, [OIII] $\lambda\lambda$ 4959, 5007 emitters at $z \approx 0.63$, $H\beta$ emitters at $z \approx 0.68$, or [OII] λ 3727 emitters at $z \approx 1.19$. In general, they are photometrically classified by using a certain broad-band color-color diagram unless

they are not strong emitters; i.e., moderate emission-line objects (e.g., Fujita et al. 2003b; Umeda et al. 2004). However, if they are very strong emitters, it becomes difficult to classify them because their strong emission lines affect their broad-band colors. In particular, as for strong *NB816*-excess objects, we cannot use I_C band photometry in such a color analysis.

We, therefore, attempt to classify strong low- z emitters by using the photometric redshift method including the effects of emission lines. Our basic method is given in Shioya et al. (2005, see also Shioya et al. 2002). To apply this method for strong emission-line galaxies, we generate SED templates with emission lines. First, we generate the continuum SEDs of model galaxies by GALAXEV (Bruzual & Charlot 2003) with adopting $\tau = 1$ Gyr. We assume Salpeter’s initial mass function (the power index of $x = 1.35$) with the stellar mass range of $0.1 \leq m/M_\odot \leq 100$. We adopt ages of $t = 2, 1, 0.1,$ and 0.01 Gyr and metallicity of $Z = 0.02, 0.008,$ and 0.004 . Second, we calculate the number of ionizing photons, $N_{\text{Ly}\alpha}$, for each SED template. We then evaluate $\text{H}\beta$ luminosity, $L(\text{H}\beta)$, using the following formula (Leitherer & Heckman 1995): $L(\text{H}\beta) = 4.76 \times 10^{-13} N_{\text{Ly}\alpha} \text{ erg s}^{-1}$. Then, we calculate emission-line ratios using Cloudy94 (Ferland 1997) for each SED template. We adopt emission-line ratios for the case of hydrogen density $n_{\text{H}} = 10^2 \text{ cm}^{-3}$, and ionization parameter $\log U = -2, -3,$ and -4 . The gas metallicity is given the same metallicity of each SED template. Finally we combine the calculated emission-line spectra with the continuum spectra for each SED template. We adopt the dust-extinction curve for starburst galaxies determined by Calzetti et al. (2000) with visual extinction of 0.0, 0.1, 0.3, 1.0, and 2.0.

Applying this photometric redshift technique, we obtain the likelihood distribution for each of our 55 strong low- z emitters as a function of redshift. The likelihood distributions are shown in right panel of figures 2 and 3. Note that the likelihood distributions are normalized by their maximum-peak value. We classify each of our emitters into three emission-line types ($\text{H}\alpha$, $\text{H}\beta$ -[OIII], and [OII]). In this classification procedure, we investigate likelihood distributions for each objects. If an emitter has a peak (or peaks) higher than 0.5 at $z \approx 0.24, z \approx 0.63$ - $0.68,$ or $z \approx 1.19,$ we classify it as an $\text{H}\alpha$, an $\text{H}\beta$ -[OIII], or an [OII] emitter, respectively. However, in some cases they are classified two or three types. Since we cannot assign a certain emission-line type to them, we call them as “possible” sample. On the other hand we call emitters with a certain type as “reliable” sample. The photometric redshifts and types of our strong low- z emitters are given in tables 3 and 4. The summary of classification is also shown in figure 4 and table 5. For reference, we also show those of LAE candidates from Ajiki et al. (2004) in figure 4 and table 5. In figure 5 we show color distributions of our strong low- z emitters. As shown in this figure, the colors of our strong low- z emitters in each emission-line type are distributed around those of the model loci. Since the distribution of observed colors of galaxies at $z = 0.24$ is very similar to that at $z = 0.63,$ usual selection by color-color diagrams cannot distinguish them. Note that possible misidentification between $\text{H}\alpha$ emitters and $\text{H}\beta$ -[OIII] emitters for galaxies with blue SEDs may be unavoidable even with our photometric redshift technique (see

section 3.6). Follow-up spectroscopic observations are necessary for exact classification.

3.5. Properties of strong low- z emitters found in our survey

We estimate the line flux (F_{line}) and observed equivalent width (EW_{obs}) of each strong low- z emitter following the method by Pascual (2001) and Fujita et al. (2003). We add the correction of the responses of filters to their methods. The flux densities (f_{ν}) in the $Iz815$, $Iz827$, $NB816$, and $IA827$ bands can be expressed as the sum of the line flux and the continuum flux densities:

$$f_{Iz815} = f_{\text{cont}} + F_{\text{line}} \frac{r_{Iz815}(\nu_{\text{line}})}{W_{Iz815}}, \quad (11)$$

$$f_{Iz827} = f_{\text{cont}} + F_{\text{line}} \frac{r_{Iz827}(\nu_{\text{line}})}{W_{Iz827}}, \quad (12)$$

$$f_{NB816} = f_{\text{cont}} + F_{\text{line}} \frac{r_{NB816}(\nu_{\text{line}})}{W_{NB816}}, \quad (13)$$

and

$$f_{IA827} = f_{\text{cont}} + F_{\text{line}} \frac{r_{IA827}(\nu_{\text{line}})}{W_{IA827}}, \quad (14)$$

where f_{cont} is the continuum flux density around the emission-line wavelength. The factors of the contributions of the line fluxes at ν_{line} to the $Iz815$, $Iz827$, $NB816$, and $IA827$ filters are denoted as $r_{Iz815}(\nu_{\text{line}})$, $r_{Iz827}(\nu_{\text{line}})$, $r_{NB816}(\nu_{\text{line}})$, and $r_{IA827}(\nu_{\text{line}})$, respectively. The values, $r_{NB816}(\nu_{\text{line}})$ and $r_{IA827}(\nu_{\text{line}})$ are equal to the responses at ν_{line} of the $NB816$ and $IA827$ filters. The values, $r_{Iz815}(\nu_{\text{line}})$ and $r_{Iz827}(\nu_{\text{line}})$, are calculated from the responses of the I_C and z' filters, $r_{I_C}(\nu_{\text{line}})$ and $r_{z'}(\nu_{\text{line}})$, as the same manner as relation (3) and (10) as follows:

$$r_{Iz815}(\nu_{\text{line}}) = 0.76r_{I_C}(\nu_{\text{line}}) + 0.24r_{z'}(\nu_{\text{line}}), \quad (15)$$

and

$$r_{Iz827}(\nu_{\text{line}}) = 0.64r_{I_C}(\nu_{\text{line}}) + 0.36r_{z'}(\nu_{\text{line}}). \quad (16)$$

The effective widths of $Iz815$, $Iz827$, $NB816$, and $IA827$ are denoted as W_{Iz815} , W_{Iz827} , W_{NB816} , and W_{IA827} , respectively. The effective width of “band”, W_{band} , is calculated from $r_{\text{band}}(\nu)$ (“band” means $Iz815$, $Iz827$, $NB816$, or $IA827$), as follows:

$$W_{\text{band}} = \int_0^{\infty} r_{\text{band}}(\nu) d\nu. \quad (17)$$

Since the ratio, $W_{\text{band}}/r_{\text{band}}(\nu)$, does not depend on the normalizing factor, we normalize $r_{\text{band}}(\nu)$ by the value averaged over effective wavelength ranges of $NB816$ (8090Å – 8210Å) for $Iz815$ and $NB816$ or those of $IA827$ (8100Å – 8440Å) for $IA827$ and $Iz827$ for convenience. By this normalization, we obtain the effective widths, $W_{Iz815} = 7.6 \times 10^{13}$ Hz, $W_{Iz827} = 8.6 \times 10^{13}$ Hz, $W_{NB816} = 6.5 \times 10^{12}$ Hz, and $W_{IA827} = 1.7 \times 10^{13}$ Hz, respectively. Then the continuum flux density, the line flux, and the equivalent width can be expressed as follows:

$$f_{\text{cont}} = \frac{f_{Iz815} - f_{NB816} \frac{W_{NB816}/r_{NB816}(\nu_{\text{line}})}{W_{Iz815}/r_{Iz815}(\nu_{\text{line}})}}{1 - \frac{W_{NB816}/r_{NB816}(\nu_{\text{line}})}{W_{Iz815}/r_{Iz815}(\nu_{\text{line}})}} \text{ for } Iz815, \quad (18)$$

$$= \frac{f_{Iz827} - f_{IA827} \frac{W_{IA827}/r_{IA827}(\nu_{\text{line}})}{W_{Iz827}/r_{Iz827}(\nu_{\text{line}})}}{1 - \frac{W_{IA827}/r_{IA827}(\nu_{\text{line}})}{W_{Iz827}/r_{Iz827}(\nu_{\text{line}})}} \text{ for } Iz827, \quad (19)$$

$$F_{\text{line}} = (f_{NB816} - f_{\text{cont}}) \frac{W_{NB816}}{r_{NB816}(\nu_{\text{line}})} \text{ for } NB816, \quad (20)$$

$$= (f_{IA827} - f_{\text{cont}}) \frac{W_{IA827}}{r_{IA827}(\nu_{\text{line}})} \text{ for } IA827, \quad (21)$$

and

$$EW_{\text{obs}} = F_{\text{line}}/f_{\text{cont}}. \quad (22)$$

In the estimates of the continuum flux densities and line fluxes, we use relations (18) and (20) for our *NB816*-selected emitters and use relations (19) and (21) for our *IA827*-selected emitters. As for the factors of the contributions of line fluxes, we use the value averaged over the effective wavelength range of *NB816* or *IA827* [i.e., $r_{\text{band}}(\nu_{\text{line}}) = 1$] since we have no information about the detailed line wavelengths of our emitters. The line fluxes, observed equivalent widths, and the FWHMs of the image sizes for our *NB816*- and *IA827*-selected emitters are given in tables 3 and 4, respectively.

The large uncertainties which is independent from photometric error possibly exists in the above estimates. For example, if a very strong emission line is at nearly the edge of the *NB816* filter response curve where the response is $\lesssim 50\%$ of the averaged value, the equivalent width and the line flux of the emitter are underestimated by a factor of $\gtrsim 2$. In addition to this, in the case of the $\text{H}\beta$ -[OIII] emitters, there are also uncertainties of the types ($\text{H}\beta$, [OIII] $\lambda 5007$, or [OIII] $\lambda 4959$) and the number of the emission lines covered by *NB816* or *IA827*. For example, for a $\text{H}\beta$ -[OIII] emitter at $z = 0.63$, we can only detect the [OIII] $\lambda 5007$ emission line by our *NB816* or *IA827* observation and miss the other ($\text{H}\beta$ and [OIII] $\lambda 4959$) emission lines. Therefore, we may underestimate EW_{obs} and F_{line} of some of our emitters by a factor of $\gtrsim 2$. In particular, the estimates of the most of the $\text{H}\beta$ -[OIII] emitters may be underestimated. The spectroscopic observation is necessary to estimate the equivalent widths and the line fluxes without these uncertainties.

We compare the estimates of EW_{obs} obtained from the *IA827* excess with those from the *NB816* excess of the four emitters (Nos. 2, 12, 31, and 41) selected as both the *NB816* and *IA827* excess. Although the two estimates are nearly the same for one object (No. 2), for the other three objects (Nos. 12, 31, and 41), the estimates from *IA827* excess are larger than those from the *NB816* excess by a factor of 2 – 3. These large differences can be explained by the uncertainty noted above. For example, if those emitters have a emission line at $\approx 8220\text{\AA}$ where the normalized response of *IA827* is higher than that of *NB816* by a factor of ≈ 2 , the estimates of EW_{obs} from *IA827* is also higher than that from *NB816* by a factor of ≈ 2 . On the other

hand, if they are $H\beta$ -[OIII] emitters, the wide passband of *IA827* can cover both $H\beta$ and [OIII] emission lines simultaneously, while the narrower wavelength coverage of *NB816* may cover only one of them (see figure 6).

We also estimate the line luminosity (L_{line}) and rest frame equivalent width (EW_0) for each strong low- z emitter using the following relations:

$$L_{\text{line}} = 4\pi d_L^2 F_{\text{line}}, \quad (23)$$

and

$$EW_0 = EW_{\text{obs}}/(1+z), \quad (24)$$

where d_L is the luminosity distance. In the above estimate, we assume $z = 0.24$, $z = 0.65$ and $z = 1.19$ for $H\alpha$, $H\beta$ -[OIII], and [OII] emitters, respectively. We also estimate the absolute B magnitude (M_B) for each of our $H\alpha$ and $H\beta$ -[OIII] emitters and the absolute magnitude at $\lambda_c \simeq 4100\text{\AA}$ (M_{410}) for each of our [OII] emitters since the central wavelength of the most redward band used in our survey, z' ($\lambda_{\text{center}} \simeq 9000\text{\AA}$), corresponds to the rest frame wavelength of $\simeq 4100\text{\AA}$ at $z \sim 1.2$. The estimates of L_{line} , EW_0 , and M_B (or M_{410}) for our strong low- z emitters are given in tables 6, 7, and 8.

3.6. Comparison with emission-line galaxies at $z < 0.1$ in the SDSS data

It is interesting to study whether or not our strong low- z emitters have common properties with those of emission-line galaxies in the local universe. For this purpose, we select the three types of emitters in the local universe from the galaxies in the spectroscopic catalog of the third data release of the SDSS (SDSS DR3; Abazajian et al. 2005). The SDSS samples are selected so as to match the absolute magnitude limits of our strong low- z emitter samples ($M_B < -13.5$ for $H\alpha$ emitters, $M_B < -16.3$ for $H\beta$ - [OIII] emitters, and $M_{410} < -17.6$ for [OII] emitters). The redshift ranges of the resultant SDSS samples are $0.003 < z < 0.006$ for $H\alpha$ emitters, $0.008 < z < 0.015$ for $H\beta$ - [OIII] emitters, and $0.03 < z < 0.06$ for [OII] emitters. The rest-frame equivalent widths of $H\alpha$, $H\beta$ - [OIII], and, [OII] emitters in the SDSS DR3 are estimated as follows:

$$EW_0 = \frac{EW_{H\alpha} + EW_{6548} + EW_{6583}}{1+z}, \quad (25)$$

$$EW_0 = \frac{EW_{H\beta} + EW_{4959} + EW_{5007}}{1+z}, \quad (26)$$

and

$$EW_0 = \frac{EW_{3726} + EW_{3729}}{1+z}, \quad (27)$$

where $EW_{H\alpha}$, EW_{6548} , EW_{6583} , $EW_{H\beta}$, EW_{4959} , EW_{5007} , EW_{3726} , and EW_{3729} are equivalent widths of $H\alpha$, [NII] λ 6548, [NII] λ 6583, $H\beta$, [OIII] λ 4959, [OIII] λ 5007, [OII] λ 3726, and [OII] λ 3729, respectively. We compare the redshift range, the survey volume, the limiting EW_0 , the numbers, and the number density of each type of emitters in the SDSS DR3 to those of our strong

low- z emitters in table 9. It is noted that approximately 10% of objects are missed from the spectroscopic catalog of the SDSS DR3 by fiber collisions. Since this incompleteness is negligibly small, we perform no correction for the detection completeness the following analysis.

In figure 7, we compare EW_0 and M_B distributions for our sample with those of the SDSS DR3. As shown in the left and right panels of this figure, the properties of M_B and EW_0 of strong H α emitters at $z \approx 0.24$ and [OII] emitters at $z \approx 1.19$ found in our survey are similar to those of the SDSS DR3. However, as shown in middle panel of the figure, some of our H β -[OIII] emitters at $z \approx 0.63$ – 0.68 are more luminous than those of the SDSS DR3. We wonder if they may be misidentified in our classification, since as mentioned before, it is often difficult distinguish between H β -[OIII] and H α emitters. If they were H α emitters at $z \sim 0.24$, their M_B could correspond to the bright part of the H α emitters in the SDSS DR3. Follow-up optical spectroscopy will be necessary to disentangle this issue.

In figure 8, we show distributions of EW_0 of the three types of emitters. Even if “possible” emitters included, the number density of our H α emitters at $z \approx 0.24$ with $EW_0 > 190\text{\AA}$ ($5.2 \times 10^{-3} \text{ Mpc}^{-3}$) is lower than that of the SDSS DR3 at $0.003 < z < 0.006$ ($1.0 \times 10^{-2} \text{ Mpc}^{-3}$). It indicates that the detection completeness of our survey for H α emitters is $\approx 52\%$ of the SDSS DR3. Note that even if all of our emitters classified as H β -[OIII] were to be H α emitters, the detection completeness of our survey for H α emitters would be $\approx 80\%$ of the SDSS DR3 at most. On the other hand, even if excluding the “possible” objects, the number density for our [OII] emitters at $z \approx 1.19$ with $EW_0 > 110\text{\AA}$ ($1.7 \times 10^{-4} \text{ Mpc}^{-3}$) is about 6 times higher than that for the SDSS DR3 at $0.03 < z < 0.06$ ($3.0 \times 10^{-5} \text{ Mpc}^{-5}$) (see the bottom panel of figure 8 or table 9). If we assume that the ratio of the detection completeness for [OII] emitters of our survey to that of the SDSS DR3 is almost the same as that for H α emitters (80% at most), the number density (or emission-line equivalent widths) of strong [OII] emitters may decrease from $z \sim 1$ to $z \sim 0$ by a factor of $\gtrsim 7$. Therefore, the number density of strong [OII] emitters shows strong evolution by a factor of $\gtrsim 6$ – 7 between $z \sim 0$ and $z \sim 1$. This evolution in the [OII] equivalent width have been reported by the spectroscopic studies (e.g., Cowie et al. 1996; Hammer et al. 1997). Although our samples have uncertainty in the detection completeness and photometric redshift, this evolution is supported by the star formation history between $z \sim 0$ and $z \sim 1$ (e.g., Tresse et al. 2002; Lilly et al. 1996).

We would like to thank both the Subaru staff members for their invaluable help and T. Hayashino for his technical help. This work was financially supported in part by the Ministry of Education, Culture, Sports, Science and Technology (Nos.10044052, and 10304013) and JSPS (Nos. 15340059, and 17253001). Data reduction/analysis was in part carried out on “sb” computer system operated by the Astronomical Data Analysis Center (ADAC) and Subaru Telescope of the National Astronomical Observatory of Japan. MA, TN, and SSS are JSPS fellows.

References

- Abazajian, K., et al. 2005, AJ, 129, 1755
- Ajiki, M., et al. 2002, ApJ, 576, L25
- Ajiki, M., et al. 2003, AJ, 126, 2091
- Ajiki, M., et al. 2004, PASJ, 56, 597
- Bruzual, A. G. & Charlot, S. 2003, MNRAS, 344, 1000
- Calzetti, D., Armus, L., Bohlin, R. C., Kinney, A. L, Koornneef, J., & Storchi-Bergmann, T. 2000, ApJ, 533, 2
- Cowie, L. L., Songaila, A., Hu, E. M., & Cohen, J. G. 1996, AJ, 112, 839
- Djorgovski, S. G., Castro, S., Stern, D., & Mahabal, A. A. 2001, ApJ, 560, L5
- Fan, X., et al. 2000, AJ, 120, 1167
- Ferland, G. J. 1997, Hazy: A Brief Introduction to CLOUDY 94.00 (Univ. Kentucky, Dept. Phys. & Astron., internal rep.)
- Fujita, S. S., et al. 2003a, AJ, 125, 13
- Fujita, S. S., et al. 2003b, ApJ, 586, L115
- Goodrich, R. W., et al. 2001, ApJ, 561, L23
- Hammer, F., Flores, H., Lilly, S. J., Crampton, D., Le Fevre, O., Rola, C., Mallen-Ornelas, G., Schade, D., & Tresse, L. 1997, 481, 49
- Hao, L., et al. 2005a, AJ, 129, 1783
- Hao, L., et al. 2005b, AJ, 129, 1795
- Hu, E. M., Cowie, L. L., Capak, P., McMahan, R. G., Hayashino, T., & Komiyama, Y. 2004, AJ, 127, 563
- Hu, E. M., McMahan, R. G., & Cowie, L. L. 1999 ApJ, 522, L9
- Iye, M., et al. 2004, PASJ, 56, 381
- Kaifu, N., et al. 2000, PASJ, 52, 1
- Leitherer, C. & Heckman, T. M. 1995, ApJS, 96, 9
- Lilly, S. J., Le Fevre, O., Hammer, F., & Crampton, D. 1996, ApJ, 460, L1
- Miyazaki, S. et al. 2002, PASJ, 54, 833
- Ouchi, M. et al. 2005, ApJ, 620, L1
- Pascual, S., Gallego, J., Aragón-Salamanca, A., & Zamorano, J. 2001, A&A, 379, 798
- Rhoads, J. E. & Malhotra, S. 2001, ApJ, 563, L5
- Shioya, Y., et al. 2002, ApJ, 576, 36
- Shioya, Y., et al. 2005, PASJ, 57, in press
- Spinrad, H. 2004, in Astrophysics Update, ed. J. W. Mason (Berlin: Springer), 155
- Stern, D., Bunker, A., Spinrad, H., & Dey, A. 2000, ApJ, 537, 73
- Taniguchi, Y., et al. 2003a, ApJ, 585, L97
- Taniguchi, Y., Shioya, Y., Fujita, S. S., Nagao, T. Murayama, T., & Ajiki, M. 2003b, Journal of the Korean Astronomical Society, 36, 123.
- Tresse, L., Maddox, S., Le Fevre, O., & Cuby, J.-G. 2002, MNRAS, 337, 369
- Umeda, K. et al. 2004, ApJ, 601, 805
- Wang, J. X., Malhotra, S., & Rhoads, J. E. 2005, ApJ, 622, L77

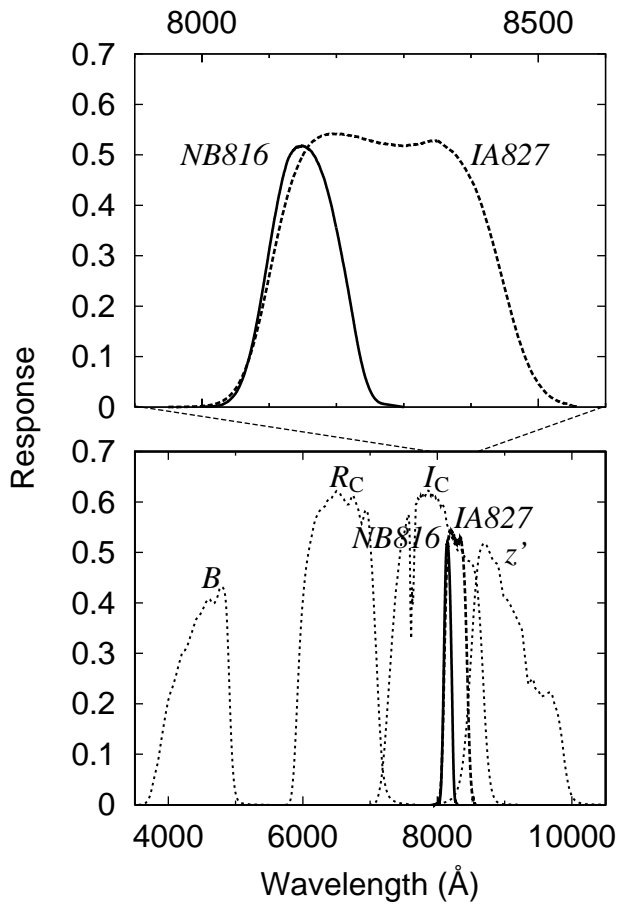


Fig. 1. Response curves (filter, optics, atmosphere transmission, and CCD sensitivity are taken into account) of the filters used in our observations. The upper panel shows the response curves of both the *NB816* and *IA827* filters.

Westra, E., Jones, D. Heath, Lidman, C. E., Athreya, R. M., Meisenheimer, K., Wolf, C., Szeifert, T.,
 Pompei, E., & Vanzi, L. 2005, *A&A*, 430, L21
 York, D. G., et al. 2000, *AJ*, 120, 1579

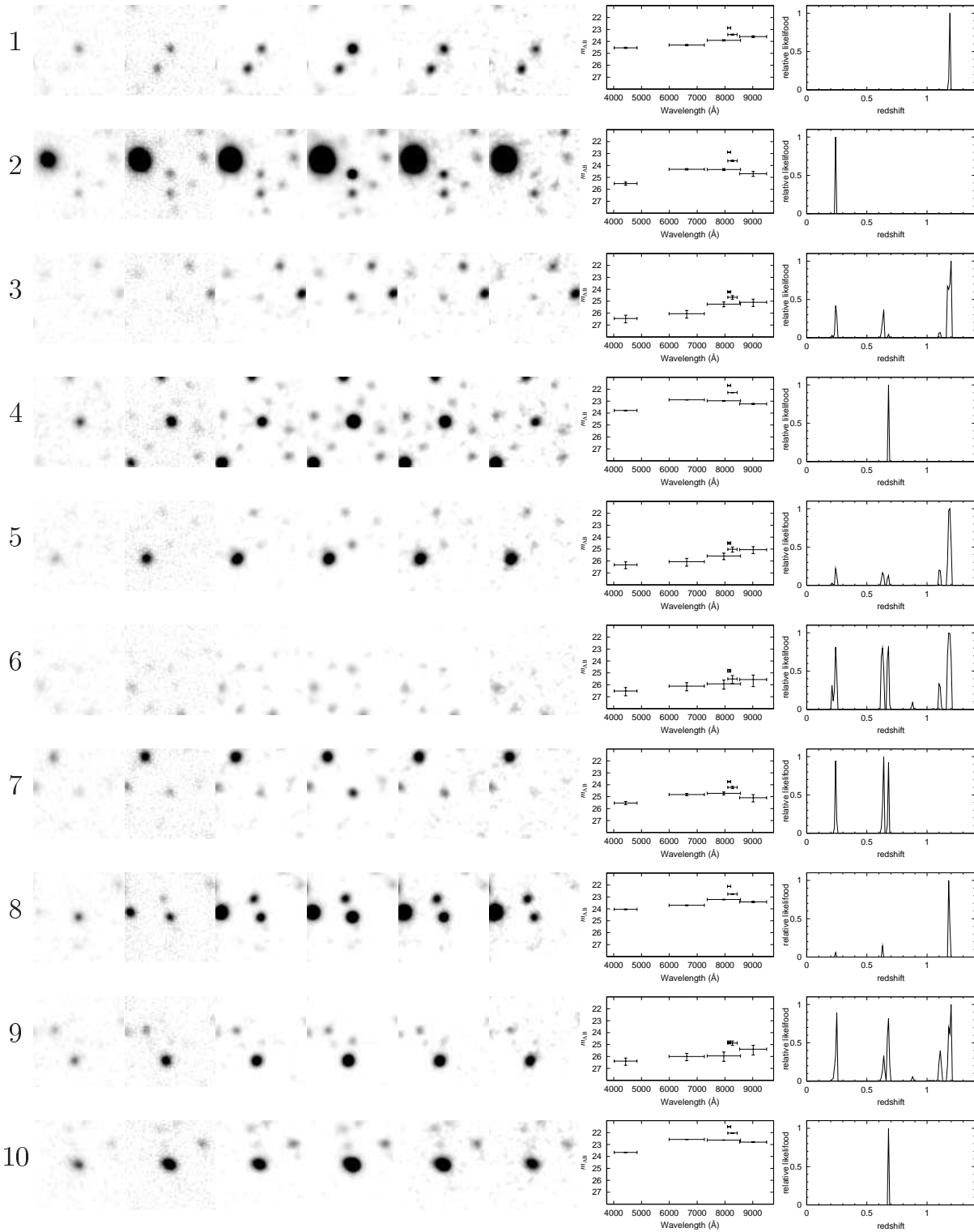
Table 1. Photometric properties of *NB816*-selected strong low-*z* emitters.

No.	α (J2000)			δ (J2000)			B^*	R_C^*	I_C^*	<i>NB816</i> *	<i>IA827</i> *	z'^*
	h	m	s	°	'	"						
1	10	43	28.0	-01	44	13	24.54	24.31	23.91	22.87	23.43	23.60
2 [†]	10	43	31.4	-01	42	36	25.52	24.32	24.34	22.88	23.61	24.69
3	10	43	31.8	-01	41	39	26.45	26.05	25.25	24.22	24.67	25.09
4	10	43	32.1	-01	17	44	23.78	22.89	22.97	21.68	22.28	23.23
5	10	43	33.0	-01	13	46	26.32	26.06	25.58	24.50	25.02	25.05
6	10	43	34.8	-01	33	19	26.52	26.11	25.92	24.82	25.51	25.56
7	10	43	35.0	-01	13	47	25.53	24.82	24.72	23.74	24.22	25.09
8	10	43	36.5	-01	41	04	24.04	23.70	23.22	22.12	22.76	23.42
9	10	43	36.9	-01	15	18	26.39	26.00	25.95	24.81	24.87	25.39
10	10	43	39.7	-01	13	39	23.66	22.57	22.63	21.51	22.04	22.80
11	10	43	42.0	-01	14	07	25.90	25.20	25.35	23.93	24.66	25.77
12 [†]	10	43	43.0	-01	35	52	26.60	26.20	25.69	24.45	24.79	25.83
13	10	43	43.5	-01	43	02	26.11	25.99	25.77	24.62	25.45	25.58
14	10	43	44.0	-01	26	06	26.60	25.93	26.19	24.75	25.43	25.50
15	10	43	45.5	-01	43	13	24.03	23.50	22.69	21.80	22.25	22.95
16	10	43	47.0	-01	21	57	26.45	26.35	25.09	24.04	24.48	24.75
17	10	43	50.3	-01	27	59	26.65	25.58	24.94	23.97	24.65	25.20
18	10	43	50.4	-01	44	35	26.87	26.36	25.97	24.98	25.51	25.74
19	10	43	57.5	-01	44	19	26.01	25.89	25.65	24.30	24.88	25.24
20	10	44	00.5	-01	15	24	25.38	25.15	24.95	23.83	24.18	24.52
21	10	44	02.2	-01	30	30	26.14	25.52	24.87	23.68	24.45	25.50
22	10	44	02.8	-01	23	49	25.82	24.77	24.35	23.38	23.83	24.59
23	10	44	07.2	-01	21	38	26.49	25.49	25.41	24.47	24.80	25.34
24	10	44	09.4	-01	29	38	26.28	26.79	25.32	24.23	25.14	25.84
25	10	44	11.5	-01	15	06	25.72	25.22	24.40	23.33	24.07	25.37
26	10	44	12.7	-01	42	36	26.74	26.18	25.85	24.82	25.27	25.49
27	10	44	17.1	-01	18	05	26.27	25.72	25.00	23.99	24.41	24.80
28	10	44	18.1	-01	27	59	23.69	22.94	22.43	21.54	22.14	22.90
29	10	44	22.2	-01	19	12	26.64	26.21	26.04	24.90	25.49	26.05
30	10	44	36.2	-01	23	44	24.27	23.53	23.10	22.25	22.62	23.45
31 [†]	10	44	36.5	-01	18	51	26.77	25.70	25.23	24.38	24.55	25.97
32	10	44	44.5	-01	34	40	26.66	25.79	25.07	24.26	24.83	26.14
33	10	44	46.8	-01	26	19	25.84	25.75	25.32	24.34	24.92	25.24
34	10	44	48.0	-01	38	27	26.22	25.65	24.31	22.98	23.91	26.29
35	10	44	51.6	-01	35	04	26.24	25.99	26.11	24.87	25.35	25.43
36	10	44	52.4	-01	13	12	25.34	24.33	23.77	22.56	23.61	24.22
37	10	44	52.7	-01	37	22	24.75	23.79	23.56	22.65	23.13	23.64
38	10	44	54.6	-01	20	15	25.07	24.25	24.12	23.21	23.68	24.36
39	10	44	56.7	-01	17	13	24.52	23.59	22.75	21.52	22.39	23.19
40	10	44	58.3	-01	25	31	25.12	24.88	24.51	23.53	23.96	24.40
41 [†]	10	45	00.6	-01	38	30	24.05	23.45	23.02	21.81	22.28	23.38
42	10	45	02.8	-01	30	53	27.38	26.44	25.78	24.64	25.38	25.79

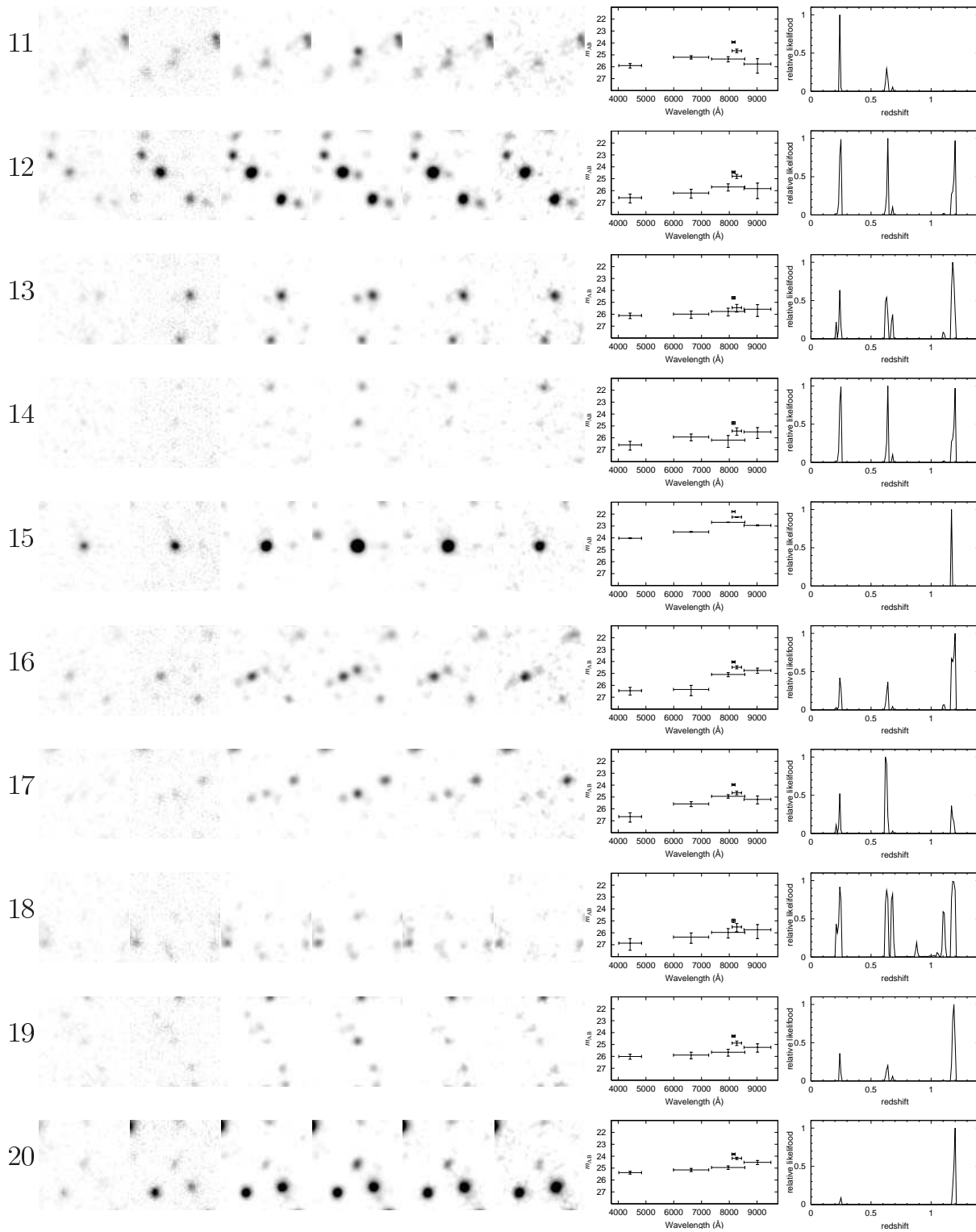
* AB magnitude in a $2''$ diameter.

[†] Objects selected both *NB816* and *IA827*.

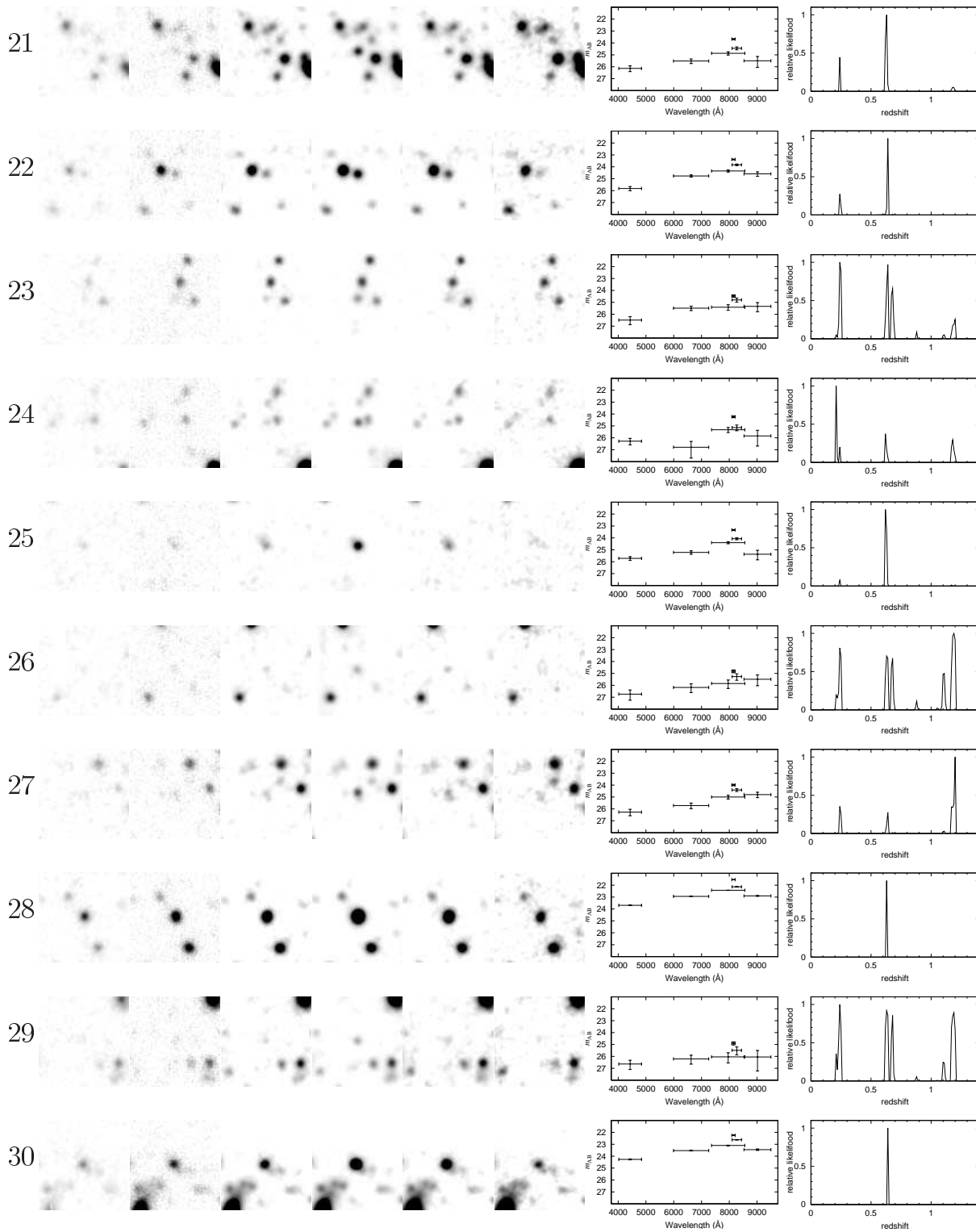
No B R_c I_c $NB816$ $IA827$ z'



No B R_c I_c $NB816$ $IA827$ z'



No B R_c I_c $NB816$ $IA827$ z'



No B R_c I_c $NB816$ $IA827$ z'

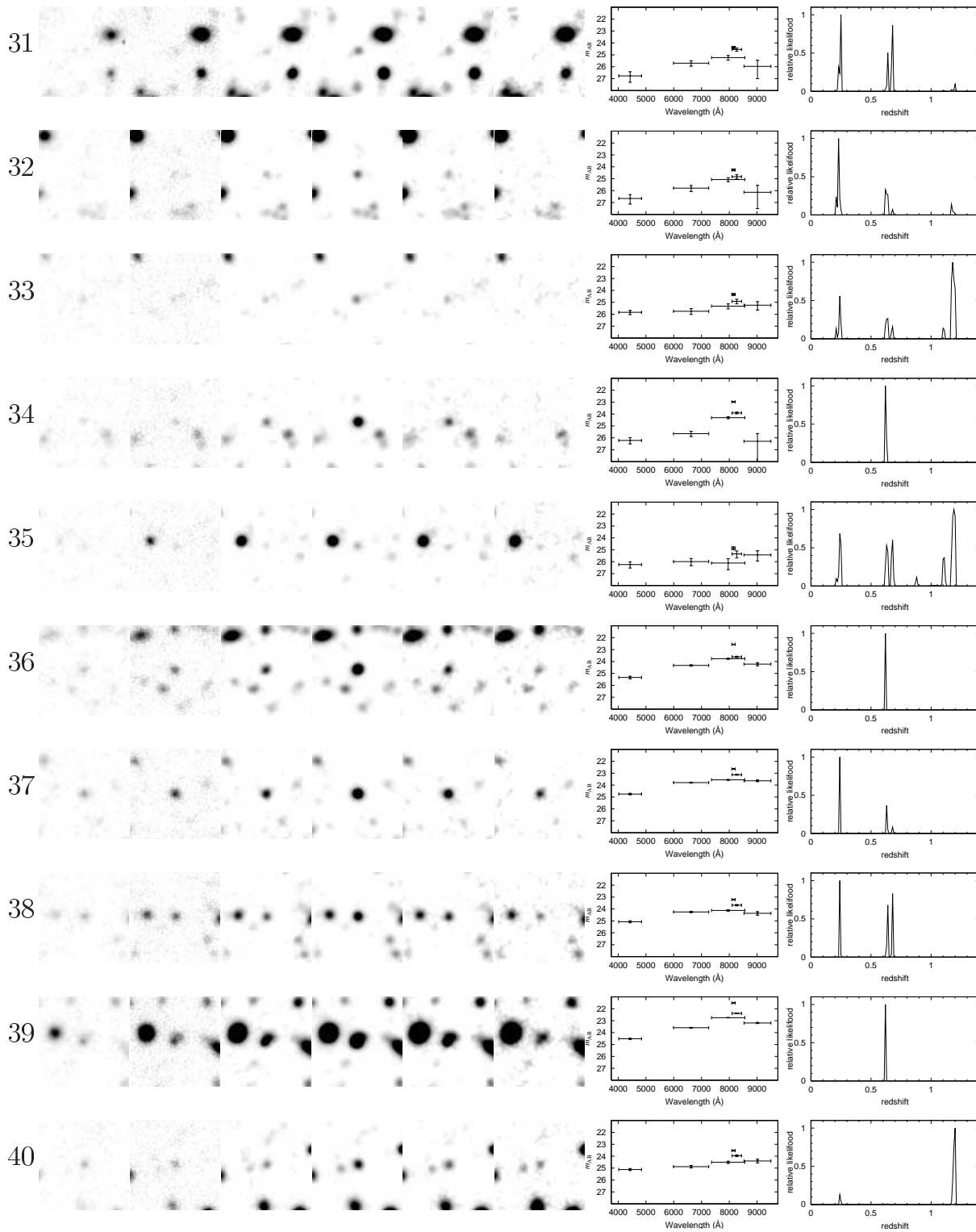


Table 2. Photometric properties of *IA827*-selected strong low-*z* emitters.

No.	α (J2000)			δ (J2000)			B^*	R_C^*	I_C^*	$NB816^*$	$IA827^*$	z'^*
	h	m	s	°	'	"						
2 [†]	10	43	31.4	-01	42	36	25.52	24.32	24.34	22.88	23.61	24.69
12 [†]	10	43	43.0	-01	35	52	26.60	26.20	25.69	24.45	24.79	25.83
31 [†]	10	44	36.5	-01	18	51	26.77	25.70	25.23	24.38	24.55	25.97
41 [†]	10	45	00.6	-01	38	30	24.05	23.45	23.02	21.81	22.28	23.38
43	10	43	34.8	-01	13	13	26.91	25.83	25.34	25.05	24.61	25.71
44	10	43	35.5	-01	23	10	26.54	26.15	25.00	25.52	24.22	25.71
45	10	43	49.4	-01	30	51	27.30	26.06	24.81	25.07	23.97	25.48
46	10	43	51.3	-01	17	21	99.00	25.37	25.42	25.62	24.73	26.00
47	10	44	05.3	-01	30	39	26.18	26.09	25.87	25.46	24.55	27.21
48	10	44	19.4	-01	14	01	27.46	25.69	25.61	25.15	24.62	25.94
49	10	44	28.6	-01	38	47	27.19	25.82	25.11	25.20	24.54	26.16
50	10	44	43.0	-01	36	35	24.42	23.73	23.21	22.47	22.49	23.62
51	10	44	51.6	-01	33	42	25.94	25.74	25.35	25.25	24.49	25.77
52	10	44	53.5	-01	13	52	27.02	25.84	25.59	25.27	24.62	25.61
53	10	44	58.7	-01	16	01	26.42	25.34	24.91	24.89	23.85	25.32
54	10	45	08.4	-01	14	22	25.30	25.22	25.49	24.93	24.74	26.43
55	10	45	08.5	-01	13	18	25.99	25.91	25.43	24.93	24.51	25.17

* AB magnitude in a $2''$ diameter.

[†] Objects selected both *NB816* and *IA827*.

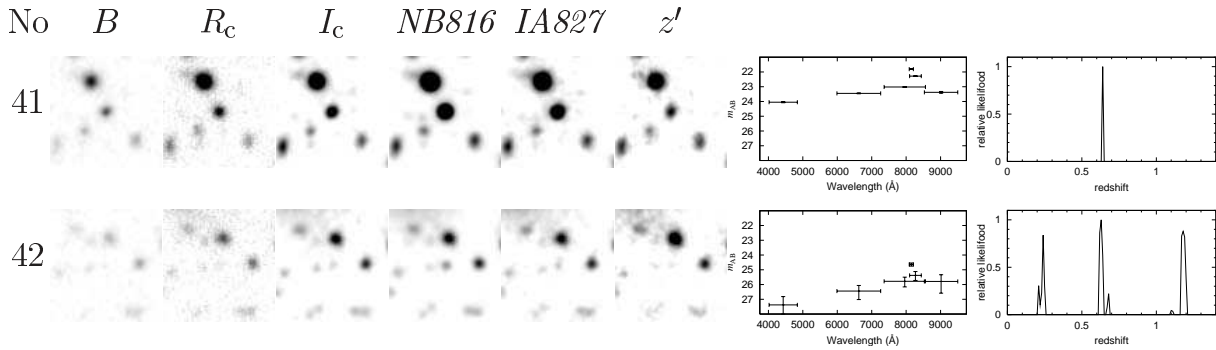


Fig. 2. B , R_C , I_C , $NB816$, $IA827$, and z' images of $NB816$ -selected strong low- z emitters. Each box is $16''$ on a side (north is up and east is left). The numbers shown in the left column correspond to those given in the first column of table 1. The SED and the likelihood distribution of each emitters are also shown in right two panels.

Table 3. Properties of *NB816*-selected strong low- z emitters.

No.	Class*	z_{ph}^{\dagger}	$FWHM_{\text{Obj}}^{\ddagger}$ (arcsec)	F_{line}^{\S} (erg s $^{-1}$ cm $^{-2}$)	$EW_{\text{obs}}^{\parallel}$ (Å)
1	[OII]	1.19	1.2	1.1×10^{-16}	258^{+26}_{-23}
2	H α	0.24	1.0	1.4×10^{-16}	700^{+118}_{-93}
3	[OII]	1.20	1.2	3.2×10^{-17}	273^{+114}_{-77}
4	H β -[OIII]	0.68	1.1	3.9×10^{-16}	501^{+21}_{-20}
5	[OII]	1.19	1.1	2.4×10^{-17}	246^{+136}_{-84}
6	([OII], H β -[OIII], H α)	1.18	1.6	1.9×10^{-17}	284^{+256}_{-124}
7	(H β -[OIII], H α)	0.64	1.1	5.2×10^{-17}	311^{+80}_{-61}
8	[OII]	1.18	1.0	2.4×10^{-16}	360^{+20}_{-18}
9	([OII], H α , H β -[OIII])	1.20	1.2	1.8×10^{-17}	269^{+233}_{-117}
10	H β -[OIII]	0.68	1.3	4.3×10^{-16}	368^{+11}_{-11}
11	H α	0.24	1.1	5.2×10^{-17}	666^{+361}_{-194}
12	(H β -[OIII], H α , [OII])	0.64	1.3	3.0×10^{-17}	448^{+341}_{-164}
13	([OII], H α , H β -[OIII])	1.18	1.2	2.4×10^{-17}	335^{+255}_{-130}
14	(H β -[OIII], H α , [OII])	0.64	1.1	2.2×10^{-17}	417^{+467}_{-183}
15	[OII]	1.17	1.0	2.9×10^{-16}	254^{+9}_{-9}
16	[OII]	1.20	1.3	3.7×10^{-17}	258^{+86}_{-63}
17	(H β -[OIII], H α)	0.62	1.0	4.1×10^{-17}	293^{+95}_{-69}
18	([OII], H α , H β -[OIII])	1.18	1.4	1.5×10^{-17}	247^{+260}_{-120}
19	[OII]	1.19	1.0	3.4×10^{-17}	423^{+250}_{-137}
20	[OII]	1.20	1.4	4.6×10^{-17}	276^{+76}_{-57}
21	H β -[OIII]	0.63	1.1	6.2×10^{-17}	479^{+146}_{-101}
22	H β -[OIII]	0.64	1.0	7.0×10^{-17}	288^{+50}_{-41}
23	(H α , H β -[OIII])	0.24	1.3	2.4×10^{-17}	241^{+129}_{-81}
24	H α	0.21	1.0	3.5×10^{-17}	387^{+198}_{-117}
25	H β -[OIII]	0.62	1.2	8.3×10^{-17}	423^{+83}_{-64}
26	([OII], H α , H β -[OIII])	1.19	1.3	1.8×10^{-17}	248^{+209}_{-108}
27	[OII]	1.20	1.3	3.9×10^{-17}	261^{+83}_{-61}
28	H β -[OIII]	0.63	1.1	3.7×10^{-16}	269^{+7}_{-8}
29	(H α , H β -[OIII], [OII])	0.24	1.1	1.8×10^{-17}	355^{+437}_{-168}
30	H β -[OIII]	0.64	1.6	1.9×10^{-16}	243^{+13}_{-13}
31	(H α , H β -[OIII])	0.25	1.7	2.7×10^{-17}	274^{+138}_{-87}
32	H α	0.23	1.0	3.1×10^{-17}	274^{+119}_{-80}
33	([OII], H α)	1.18	1.6	2.8×10^{-17}	258^{+120}_{-79}
34	H β -[OIII]	0.62	1.0	1.3×10^{-16}	740^{+145}_{-110}
35	([OII], H α , H β -[OIII])	1.19	1.0	1.8×10^{-17}	298^{+302}_{-136}
36	H β -[OIII]	0.62	1.1	1.7×10^{-16}	465^{+44}_{-38}
37	H α	0.24	1.0	1.3×10^{-16}	245^{+20}_{-18}
38	(H α , H β -[OIII])	0.24	1.0	7.9×10^{-17}	260^{+37}_{-32}
39	H β -[OIII]	0.62	1.3	4.5×10^{-16}	484^{+17}_{-16}
40	[OII]	1.20	1.1	5.9×10^{-17}	258^{+50}_{-41}
41	H β -[OIII]	0.64	1.0	3.4×10^{-16}	455^{+20}_{-20}
42	(H β -[OIII], [OII], H α)	0.63	1.0	2.4×10^{-17}	358^{+296}_{-142}

* Emission line type. Possible types are put in parentheses.

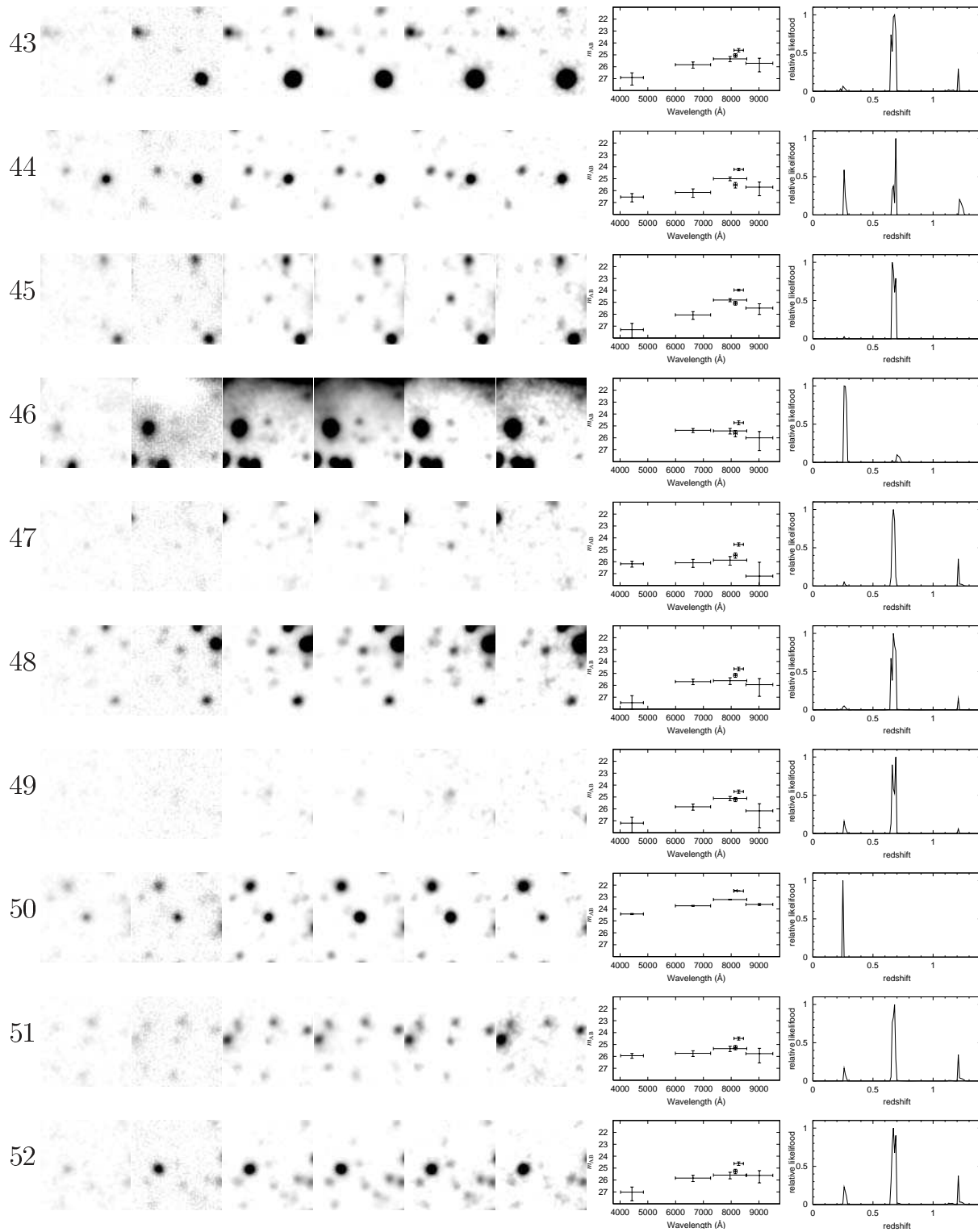
† Photometric redshift.

‡ FWHM size in the *NB816* image. The FWHM sizes of stellar objects in the *NB816* image are 0''.9.

§ Photometric error is $\approx 5 \times 10^{-18}$ erg s $^{-1}$ cm $^{-2}$.

|| Error shows only the uncertainty of photometry.

No B R_c I_c $NB816$ $IA827$ z'



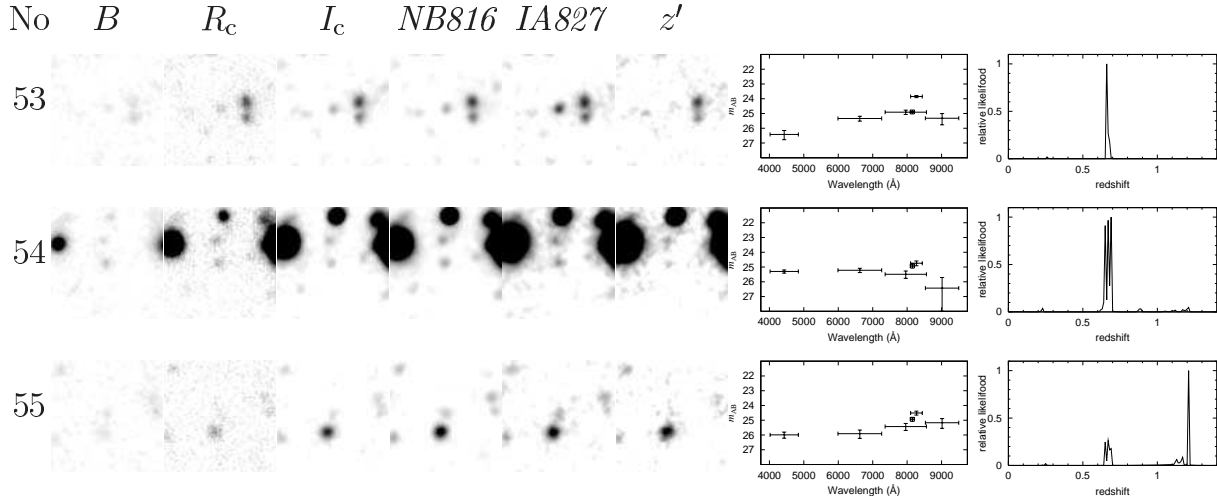


Fig. 3. B , R_c , I_c , $NB816$, $IA827$, and z' images of $IA827$ -selected strong low- z emitters. Each box is $16''$ on a side. The numbers shown in the left column correspond to those given in the first column of table 2. The SED and likelihood of each emitters are also shown in right two panels. Images of common objects, No. 2, No. 12, No. 31, and No. 41, are shown in figure 2 (see also table 2).

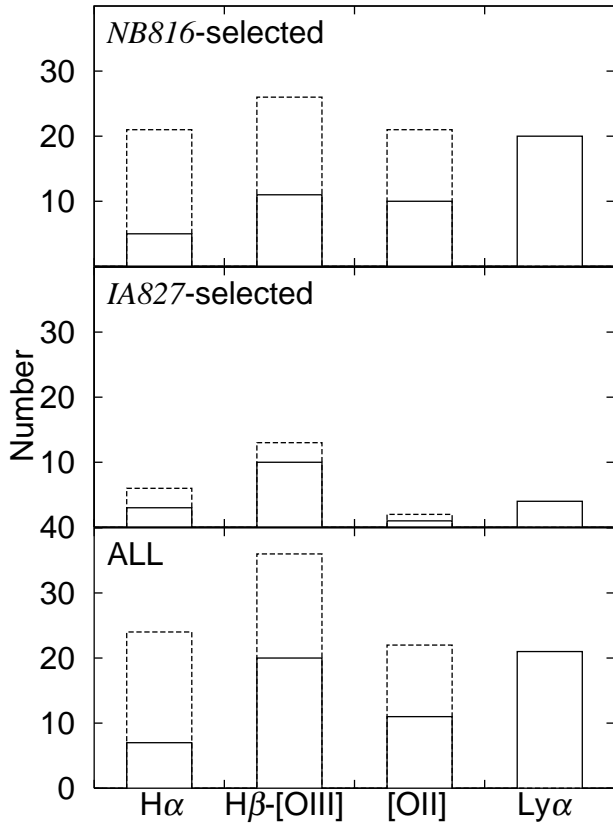


Fig. 4. Frequency distributions of emission-line objects. The solid lines show our reliable sample and dashed lines show reliable and possible sample.

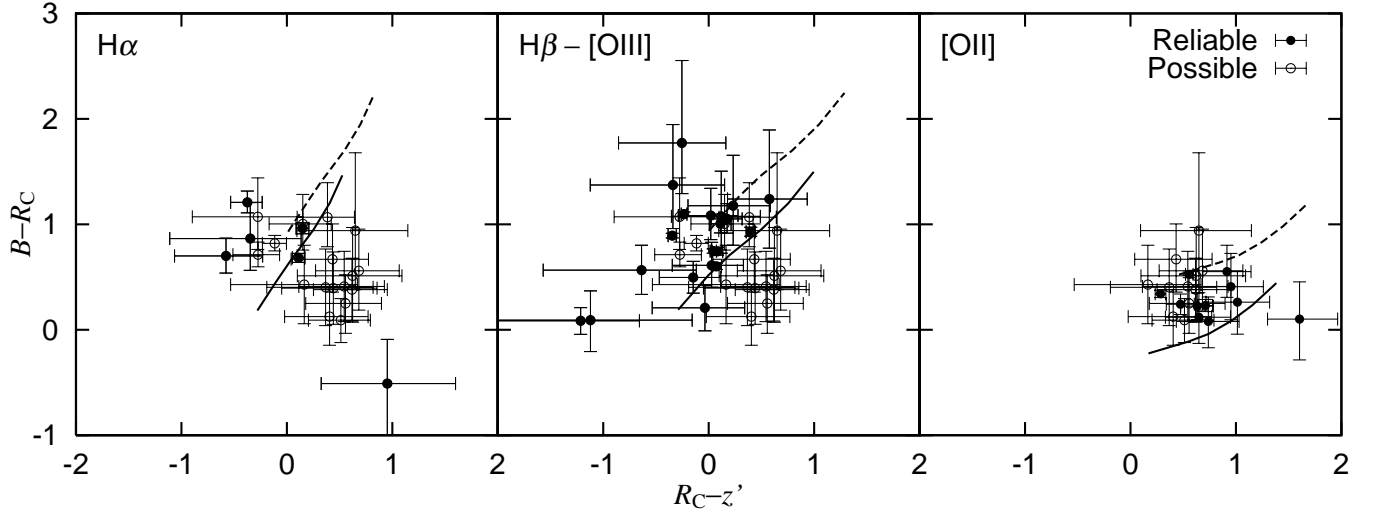


Fig. 5. Diagrams of our strong low- z emitters (left: $H\alpha$; center: $H\beta - [OIII]$; right: $[OII]$) between $B - R_C$ and $R_C - z'$. The lines are expected colors of the various age of no emission-line galaxies ($t = 2 - 0.01$ Gyr) with and metallicity of $Z = 0.02$ at $z = 0.24$ (left), $z = 0.63$ (center), and $z = 1.19$ (right). The solid and dash lines show the case of $A_V = 0$ and $A_V = 1$, respectively.

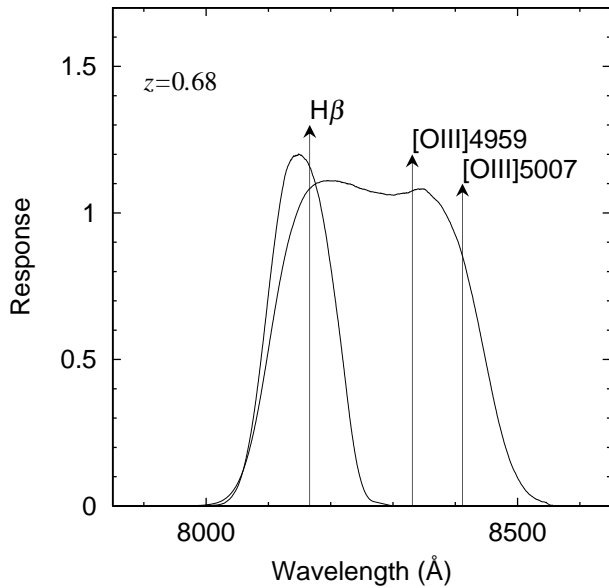


Fig. 6. Emission-line positions in cases of $H\beta - [OIII]$ emitters at $z = 0.68$ compared with normalized-response curves of *NB816* and *IA827* filter.

Table 4. Properties of *IA827*-selected strong low- z emitters.

No.	Class*	z_{ph}^{\dagger}	$FWHM_{\text{obj}}^{\ddagger}$ (arcsec)	F_{line}^{\S} ($\text{erg s}^{-1} \text{ cm}^{-2}$)	$EW_{\text{obs}}^{\parallel}$ (\AA)
2	(H β -[OIII], H α , [OII])	0.64	1.3	1.5×10^{-16}	780^{+223}_{-168}
12	(H α , H β -[OIII])	0.25	1.8	5.5×10^{-17}	802^{+861}_{-390}
31	H β -[OIII]	0.64	1.5	6.3×10^{-17}	896^{+876}_{-405}
41	(H β -[OIII], [OII], H α)	0.63	1.3	4.9×10^{-16}	779^{+59}_{-55}
43	H β -[OIII]	0.68	1.8	5.8×10^{-17}	783^{+746}_{-362}
44	(H β -[OIII], H α)	0.69	1.4	9.2×10^{-17}	1086^{+754}_{-398}
45	H β -[OIII]	0.66	1.2	1.2×10^{-16}	1214^{+665}_{-383}
46	H α	0.26	1.6	5.2×10^{-17}	800^{+927}_{-403}
47	H β -[OIII]	0.67	1.4	8.7×10^{-17}	$10000^{+\infty}_{-7946}$
48	H β -[OIII]	0.67	2.0	6.7×10^{-17}	1386^{+2402}_{-697}
49	H β -[OIII]	0.69	3.5	6.1×10^{-17}	750^{+641}_{-331}
50	H α	0.25	1.2	4.1×10^{-16}	777^{+72}_{-65}
51	H β -[OIII]	0.68	1.5	7.2×10^{-17}	1087^{+1117}_{-480}
52	H β -[OIII]	0.67	1.7	6.2×10^{-17}	1042^{+1280}_{-500}
53	H β -[OIII]	0.66	1.8	1.4×10^{-16}	1781^{+1163}_{-584}
54	H β -[OIII]	0.69	2.2	5.7×10^{-17}	1112^{+1797}_{-579}
55	H α	0.24	2.8	6.2×10^{-17}	713^{+568}_{-307}

* Emission line type. Possible types are put in parentheses.

\dagger Photometric redshift.

\ddagger FWHM size in the *IA827* image. The FWHM sizes of stellar objects in the *IA827* image are $1''.2$.

\S Photometric error is $\approx 1.7 \times 10^{-17} \text{ erg s}^{-1} \text{ cm}^{-2}$.

\parallel Error shows only the uncertainty of photometry.

Table 5. Classification of our emitters.

type		number			
		<i>NB816</i>	<i>IA827</i>	common	total
$H\alpha$	reliable	5	3	1	7
	possible	16	3	2	17
	all	21	6	3	24
$H\beta$ -[OIII]	reliable	11	10	1	20
	possible	15	3	2	16
	all	26	13	3	36
[OII]	reliable	10	1	0	11
	possible	11	1	1	11
	all	21	2	1	22
$Ly\alpha$		20	4	3	21

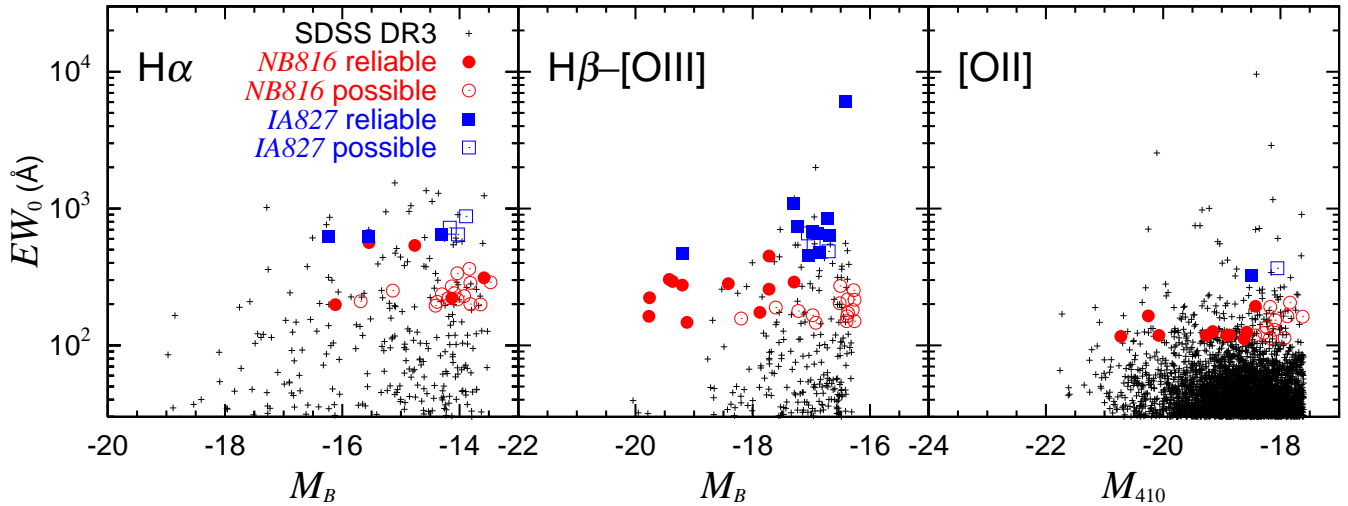


Fig. 7. Diagrams of EW_0 vs. M_B or M_{410} for our $H\alpha$ (left), $H\beta - [OIII]$ (center), and $[OII]$ (right) emitters. We also show those in the SDSS DR3 catalog for the comparison.

Table 6. EW and luminosity properties of H α emitters.

No.	L_{line}^* (erg s $^{-1}$)	EW_0^\dagger (Å)	M_B
<i>NB816</i> – reliable			
2	2.4×10^{40}	564_{-74}^{+94}	-15.5
11	9.0×10^{39}	537_{-156}^{+290}	-14.8
24	6.0×10^{39}	312_{-94}^{+159}	-13.6
32	5.3×10^{39}	220_{-63}^{+96}	-14.1
37	2.2×10^{40}	197_{-14}^{+15}	-16.1
<i>IA827</i> – reliable			
2	2.5×10^{40}	629_{-135}^{+178}	-14.1
46	9.0×10^{39}	645_{-324}^{+748}	-16.2
50	7.0×10^{40}	626_{-52}^{+57}	-14.9
<i>NB816</i> – possible			
6	3.2×10^{39}	229_{-99}^{+206}	-13.9
7	8.9×10^{39}	250_{-49}^{+64}	-15.1
9	3.2×10^{39}	216_{-93}^{+188}	-14.0
12	5.1×10^{39}	361_{-132}^{+274}	-13.8
13	4.1×10^{39}	270_{-104}^{+206}	-14.1
14	3.8×10^{39}	336_{-147}^{+376}	-14.0
17	7.1×10^{39}	236_{-55}^{+76}	-14.3
18	2.6×10^{39}	199_{-96}^{+209}	-13.6
23	4.2×10^{39}	194_{-65}^{+103}	-14.4
26	3.0×10^{39}	200_{-87}^{+168}	-13.8
29	3.2×10^{39}	286_{-135}^{+352}	-13.8
31	4.7×10^{39}	220_{-70}^{+111}	-14.2
33	4.8×10^{39}	208_{-63}^{+97}	-14.4
35	3.1×10^{39}	240_{-109}^{+243}	-14.1
38	1.4×10^{40}	209_{-25}^{+29}	-15.7
42	4.1×10^{39}	288_{-115}^{+238}	-13.5
<i>IA827</i> – possible			
12	9.4×10^{39}	646_{-314}^{+694}	-13.9
31	1.1×10^{40}	722_{-326}^{+705}	-13.8
44	1.6×10^{40}	875_{-320}^{+608}	-14.1

* Photometric error is $\approx 8 \times 10^{38}$ erg s $^{-1}$ for *NB816* and $\approx 3.0 \times 10^{39}$ erg s $^{-1}$ for *IA827*.

† The error shows only the uncertainty of photometry.

Table 7. EW and luminosity properties of H β – [OIII] emitters.

No.	L_{line}^* (erg s $^{-1}$)	EW_0^\dagger (Å)	M_B
<i>NB816</i> – reliable			
4	6.7×10^{41}	303^{+12}_{-12}	-19.4
10	7.4×10^{41}	223^{+6}_{-6}	-19.8
21	1.1×10^{41}	290^{+88}_{-61}	-17.3
22	1.2×10^{41}	174^{+30}_{-25}	-17.9
25	1.4×10^{41}	256^{+49}_{-39}	-17.7
28	6.4×10^{41}	163^{+4}_{-4}	-19.8
30	3.2×10^{41}	147^{+8}_{-7}	-19.1
34	2.2×10^{41}	448^{+87}_{-66}	-17.7
36	2.9×10^{41}	281^{+26}_{-23}	-18.4
39	7.8×10^{41}	293^{+10}_{-9}	-19.4
41	5.9×10^{41}	275^{+11}_{-12}	-19.2
<i>IA827</i> – reliable			
41	8.5×10^{41}	472^{+35}_{-33}	-17.0
43	1.0×10^{41}	474^{+452}_{-219}	-16.4
45	2.0×10^{41}	735^{+403}_{-232}	-17.0
47	1.5×10^{41}	$6060^{+\infty}_{-4815}$	-16.9
48	1.2×10^{41}	840^{+1455}_{-422}	-16.7
49	1.0×10^{41}	454^{+387}_{-200}	-17.3
51	1.2×10^{41}	658^{+676}_{-290}	-16.8
52	1.1×10^{41}	631^{+775}_{-303}	-18.0
53	2.5×10^{41}	1079^{+704}_{-353}	-16.7
54	9.8×10^{40}	673^{+1088}_{-350}	-17.0
<i>NB816</i> – possible			
6	3.2×10^{40}	172^{+155}_{-75}	-16.4
7	9.0×10^{40}	188^{+48}_{-36}	-17.6
9	3.2×10^{40}	163^{+141}_{-70}	-16.4
12	5.1×10^{40}	271^{+206}_{-99}	-16.5
13	4.1×10^{40}	203^{+155}_{-78}	-16.5
14	3.8×10^{40}	252^{+282}_{-110}	-16.3
17	7.1×10^{40}	177^{+57}_{-41}	-17.2
18	2.6×10^{40}	149^{+157}_{-72}	-16.3
23	4.2×10^{40}	146^{+78}_{-49}	-16.9
26	3.1×10^{40}	150^{+126}_{-65}	-16.4
29	3.2×10^{40}	215^{+264}_{-101}	-16.3
31	4.7×10^{40}	166^{+83}_{-52}	-17.0
35	3.1×10^{40}	180^{+183}_{-82}	-16.3
38	1.4×10^{41}	157^{+22}_{-19}	-18.2
42	4.1×10^{40}	216^{+179}_{-86}	-16.4
<i>IA827</i> – possible			
12	9.5×10^{40}	486^{+521}_{-236}	-17.1
31	1.1×10^{41}	543^{+530}_{-245}	-17.2
44	1.6×10^{41}	658^{+457}_{-241}	-16.7

* Photometric error is $\approx 8 \times 10^{39}$ erg s $^{-1}$ for *NB816* and $\approx 3.0 \times 10^{40}$ erg s $^{-1}$ for *IA827*.

† The error shows only the uncertainty of photometry.

Table 8. EW and luminosity properties of [OII] emitters.

No.	L_{line}^* (erg s ⁻¹)	EW_0^\dagger (Å)	M_{410}
<i>NB816</i> – reliable			
1	8.7×10^{41}	117_{-10}^{+11}	-20.1
3	2.6×10^{41}	124_{-35}^{+52}	-18.6
5	1.9×10^{41}	112_{-38}^{+62}	-18.6
8	1.9×10^{42}	164_{-8}^{+8}	-20.3
15	2.3×10^{42}	115_{-4}^{+4}	-20.7
16	3.0×10^{41}	117_{-28}^{+39}	-18.9
19	2.7×10^{41}	193_{-62}^{+114}	-18.4
20	3.7×10^{41}	126_{-26}^{+34}	-19.2
27	3.1×10^{41}	119_{-27}^{+37}	-18.9
40	4.8×10^{41}	117_{-18}^{+22}	-19.3
<i>IA827</i> – reliable			
55	4.9×10^{41}	325_{-140}^{+259}	-20.3
<i>NB816</i> – possible			
6	1.5×10^{41}	129_{-56}^{+117}	-18.1
9	1.5×10^{41}	122_{-53}^{+106}	-18.3
12	2.4×10^{41}	204_{-74}^{+155}	-17.8
13	1.9×10^{41}	152_{-59}^{+116}	-18.1
14	1.8×10^{41}	190_{-83}^{+213}	-18.2
18	1.2×10^{41}	112_{-54}^{+118}	-17.9
26	1.4×10^{41}	113_{-49}^{+95}	-18.2
29	1.5×10^{41}	162_{-76}^{+199}	-17.6
33	2.2×10^{41}	117_{-36}^{+55}	-18.4
35	1.4×10^{41}	136_{-61}^{+138}	-18.2
42	1.9×10^{41}	163_{-65}^{+134}	-17.9
<i>IA827</i> – possible			
12	4.4×10^{41}	366_{-177}^{+393}	-18.0

* Photometric error is $\approx 4 \times 10^{40}$ erg s⁻¹ for *NB816* and $\approx 1.4 \times 10^{41}$ erg s⁻¹ for *IA827*.

† The error shows only the uncertainty of photometry.

Table 9. EW and luminosity properties of *NB816*-selected strong low- z emitters.

catalog	redshift range	volume (Mpc ³)	$EW_{0,\text{lim}}$ Å	M_{lim}^*	Number [†]	Number density [†] (Mpc ⁻³)
H α						
<i>NB816</i>	0.23 – 0.25	4.0×10^3	≈ 190	$M_B \approx -13.5$	5–21	$1.2\text{--}5.2 \times 10^{-3}$
<i>IA827</i>	0.23 – 0.29	1.1×10^4	≈ 550	$M_B \approx -13.5$	3–6	$2.7\text{--}5.4 \times 10^{-4}$
SDSS DR3	0.003 – 0.006	6.3×10^3	190	$M_B = -13.5$	62	1.0×10^{-2}
SDSS DR3	0.003 – 0.006	6.3×10^3	550	$M_B = -13.5$	18	3.2×10^{-3}
H β –[OIII]						
<i>NB816</i>	0.62 – 0.69	6.6×10^4	≈ 140	$M_B \approx -16.3$	11–26	$1.7\text{--}4.0 \times 10^{-4}$
<i>IA827</i>	0.62 – 0.73	1.3×10^5	≈ 410	$M_B \approx -16.3$	10–13	$7.6\text{--}10 \times 10^{-5}$
SDSS DR3	0.008 – 0.015	9.5×10^4	140	$M_B = -16.3$	55	5.5×10^{-4}
SDSS DR3	0.008 – 0.015	9.5×10^4	410	$M_B = -16.3$	13	1.3×10^{-4}
[OII]						
<i>NB816</i>	1.17 – 1.20	6.0×10^5	≈ 110	$M_{410} \approx -17.6$	10–21	$1.7\text{--}3.5 \times 10^{-4}$
<i>IA827</i>	1.17 – 1.26	1.7×10^6	≈ 310	$M_{410} \approx -17.6$	1–2	$5.9\text{--}12 \times 10^{-7}$
SDSS DR3	0.03 – 0.06	6.0×10^6	110	$M_{410} = -17.6$	178	3.0×10^{-5}
SDSS DR3	0.03 – 0.06	6.0×10^6	310	$M_{410} = -17.6$	22	3.3×10^{-6}

* Limiting absolute magnitude.

† The cases for only reliable sample and all (reliable and possible) sample are shown as the minimum and maximum values, respectively.

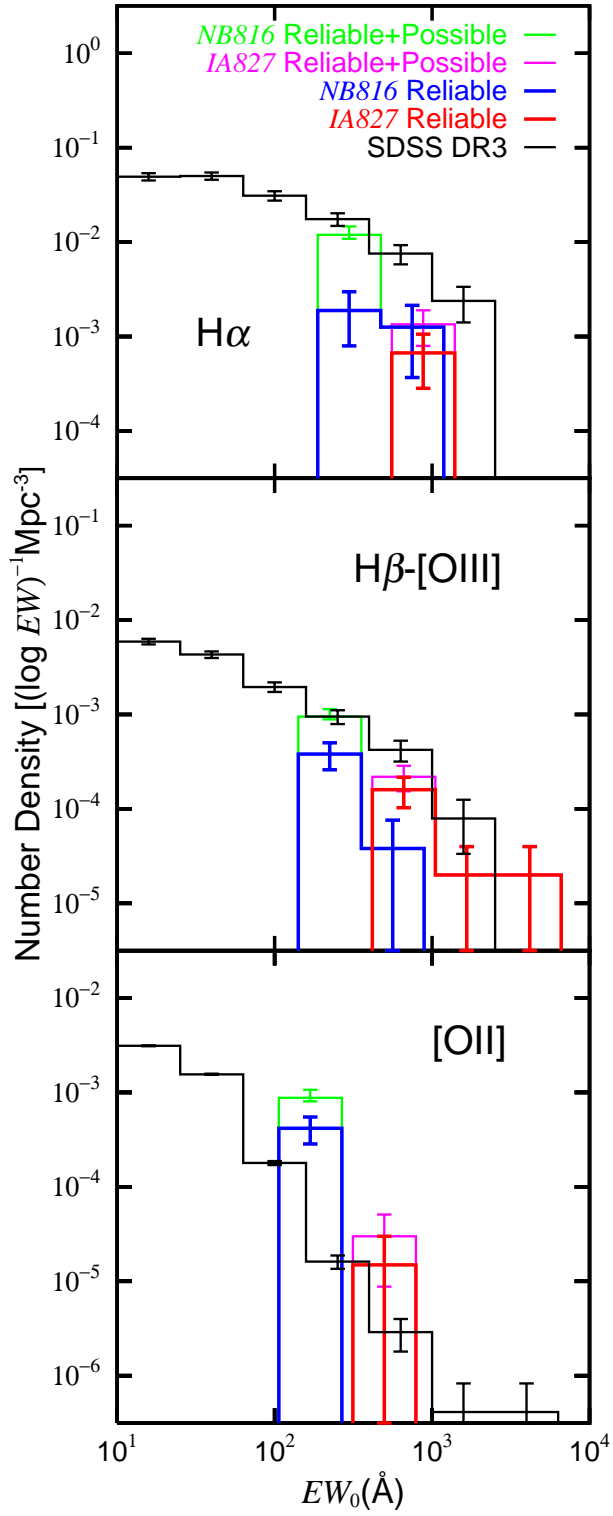


Fig. 8. Distributions of EW_0 for our $H\alpha$ (top), $H\beta - [OIII]$ (center), and $[OII]$ (bottom) emitters. We also show those in the SDSS DR3 catalog for the comparison.